

# Rigorous renormalization group method for ground space and low-energy states of local Hamiltonians

Brenden Roberts,\* Thomas Vidick, and Olexei I. Motrunich

*Institute for Quantum Information and Matter,  
California Institute of Technology, Pasadena, CA 91125*

(Dated: June 15, 2022)

The practical success of polynomial-time tensor network methods for computing ground states of certain quantum local Hamiltonians has recently been given a sound theoretical basis by Arad *et al.*<sup>1</sup>. The convergence proof, however, relies on “rigorous renormalization group” (RRG) techniques which differ fundamentally from existing algorithms. We introduce an efficient implementation of the theoretical RRG procedure which finds MPS ansatz approximations to the ground spaces and low-lying excited spectra of local Hamiltonians in situations of practical interest. In contrast to other schemes, RRG does not utilize variational methods on tensor networks. Rather, it operates on subsets of the system Hilbert space by constructing approximations to the global ground space in a tree-like manner. We evaluate the algorithm numerically, finding similar performance to DMRG in the case of a gapped nondegenerate Hamiltonian. Even in challenging situations of criticality, or large ground-state degeneracy, or long-range entanglement, RRG remains able to identify candidate states having large overlap with ground and low-energy eigenstates, outperforming DMRG in some cases.

## I. INTRODUCTION

Many important techniques for solving lattice models in condensed matter physics take the form of tensor network algorithms. The seminal such method is White’s density matrix renormalization group (DMRG),<sup>2</sup> an optimization algorithm on the matrix product state (MPS) ansatz of quantum wavefunctions<sup>3,4</sup> developed as a controllable method improving on Wilson’s numerical renormalization group for impurity systems.<sup>5</sup> DMRG remains the most versatile procedure in its class. It has been heavily used to numerically solve low-dimensional quantum models; an early example is the Haldane phase in the Heisenberg chain.<sup>6</sup> More recently, a related approach was used in the classification of all gapped phases in one dimension.<sup>7</sup> Other related techniques include the tensor renormalization group and tensor network renormalization, which utilize a two-dimensional coarse-graining process to solve quantum systems in one dimension by the quantum-to-classical correspondence.<sup>8–10</sup> Other variational algorithms operate on the multiscale entanglement renormalization ansatz (MERA), which efficiently represents states exhibiting a logarithmic violation of the area law by encoding correlations at all scales in an optimized quantum circuit of logarithmic depth.<sup>11–15</sup>

In this paper, we present an alternative approach to the solution of local Hamiltonians in one dimension (1D). The rigorous renormalization group (RRG) is a recent algorithm developed as part of a proof of the tractability of computing ground states of gapped local Hamiltonians in 1D.<sup>1,16</sup> The proof develops a set of techniques first introduced to establish an improved one-dimensional area law.<sup>17</sup> Broadly, RRG operates on states in the Hilbert spaces associated with blocks of sites, identifying sets of states based on a certain condition indicating that they are extendable in the full Hilbert space to a good approximation of the Hamiltonian’s low-energy eigenspace.

In the algorithm these are called “viable sets,” and are merged on adjoining regions in a hierarchical tree-like fashion in order to generate a subspace supported on the whole system that is close to the global low-energy space.

In the present work we adapt these techniques to specify a concrete RRG procedure allowing for the explicit computation of approximations to ground states of local Hamiltonians. This requires making allowance for computational limitations, and generally our modifications operate outside of the regime of rigorous guarantee. Still, our algorithm presents a conceptually new approach to this task.

The main conceptual departure of this algorithm from existing tensor network methods is that RRG operates on the viable sets, rather than on variational states on the full Hilbert space. Two important features arise from this distinction. First, no local optimization step is performed to minimize the energy of a particular ansatz state. Even though in the RRG procedure described here the basic operations are performed on MPS comprising an approximate basis of the viable sets, the MPS objects themselves are incidental, and the concerns arising from the MPS ansatz (*e.g.*, gauge choice, truncation) are external to the fundamental algorithm.

Second, the physical degrees of freedom are not subject to coarse-graining. Usually the objective of a coarse-graining strategy is to limit the dimensionality of the Hilbert space at increasing scale by the introduction of renormalized degrees of freedom, as determined by some local rule. The effective Hilbert space for such degrees of freedom corresponds to some subset of the original space, often having constant dimension at all scales. Instead of this, RRG performs an analogous process by maintaining viable sets of constant dimension at all levels of the algorithm hierarchy. These processes cannot be considered equivalent, as RRG includes a step of applying an “approximate projection” operator, which is specified on

the full Hilbert space. This changes the relationship between viable sets at different scales in a complicated way, and does not match the intuition of an “RG flow” in a small number of parameters. However, this method still allows for fully controllable systematic improvements in accuracy.

The structure of this paper is as follows. We first give a detailed, self-contained description of our algorithm in Sec. II. (We refer the reader familiar with the theoretical RRG paper to App. A for a precise discussion of the differences between the proof and the present work.) We provide an extended discussion of numerical results in Sec. III. Given its origins as a highly technical theoretical algorithm developed in order to obtain provable guarantees, the RRG method performs surprisingly well, often matching the results of DMRG and outperforming it in certain difficult cases exhibiting degenerate ground spaces or highly entangled ground states. Finally, we conclude and give directions for further work in Sec. IV.

## II. OPERATION OF ALGORITHM

### A. Overview and notation

The steps comprising the RRG as implemented are listed in Fig. 1 for reference and are discussed in detail in subsequent sections. A visual schematic of the algorithm is shown in Fig. 2. We will use the following notation. Let  $H = \sum_{i=0}^{N-2} h_i$  be a 2-local Hamiltonian on a chain of  $N$  qubits, with term  $h_i$  acting on sites  $i$  and  $i + 1$ . (The generalization to  $k$ -local Hamiltonians and qudits is straightforward.) Denote the Hilbert space of the system by  $\mathfrak{H}$ , and refer to the low-energy eigenspace of  $H$  as  $T$ . Let  $n$  be a parameter specifying the size of initial regions of the system, and assume  $N/n$  is a power of 2. For each  $m = 0, 1, \dots, \log_2(N/n)$ , partition the  $N$ -site system into contiguous blocks of equal length  $2^m n$ . Call these  $J_m^\lambda = \{\lambda 2^m n, \dots, (\lambda + 1) 2^m n - 1\}$ , for  $\lambda = 0, 1, \dots, N/(2^m n) - 1$ . The Hilbert space associated with  $J_m^\lambda$  is denoted  $\mathfrak{H}_m^\lambda$ , and  $\mathfrak{H} = \bigotimes_\lambda \mathfrak{H}_m^\lambda$ . Let  $H_m^\lambda$  be the block Hamiltonian on  $J_m^\lambda$ , comprising all terms acting only on sites in  $J_m^\lambda$  and excluding boundary terms. Explicitly,  $H_m^\lambda = \sum_{i \in J_m^\lambda} h_i$ , where  $J_m^{\lambda*} = \{\lambda 2^m n, \dots, (\lambda + 1) 2^m n - 2\}$ .

### B. Initialization

The first step is to construct an *approximate ground state projector* (AGSP)  $K$ , whose action on states in  $\mathfrak{H}$  increases overlap with  $T$ , the low-energy subspace of  $H$ . Many constructions of AGSP are possible. In the interest of efficiency, we use an AGSP obtained as an approximation to a thermal operator at temperature  $t/k$ ,  $K \approx e^{-kH/t}$ ,  $t, k > 0$ . Let  $Q_t$  denote a matrix product operator (MPO) approximating the thermal opera-

tor  $e^{-H/t}$  at temperature  $t$ ; procedures such as a Trotter decomposition<sup>18</sup> or cluster expansion can be used to efficiently compute this MPO. The AGSP is then obtained as a power of  $Q_t$ , contracting the product on the physical indices  $k$  times.

The computation of  $Q_t$  involves contraction of a tensor network consisting of terms of the form  $e^{-h_i/t}$ . After each contraction an SVD is performed between site indices, and the MPO is truncated by eliminating low-weight Schmidt vectors across each bond. Here truncation is meant in the sense of MPS truncation, representing the MPO as a state in a higher-dimensional local Hilbert space. This amounts to using the Frobenius norm to order the terms in the sum arising from the SVD, and may not be an optimal way to approximate operators; we will discuss this issue in more detail later.

The second step in the initialization is to identify sets of states  $V_0^\lambda \subset \mathfrak{H}_0^\lambda$ , for  $\lambda = 0, 1, \dots, N/n - 1$ , of constant dimension  $s$ , where  $s$  is a parameter of the algorithm which bounds the dimension of the sets manipulated throughout. We use the term “viable sets” for the  $V_0^\lambda$  (generally, for  $V_m^\lambda \subset \mathfrak{H}_m^\lambda$ ) because the intent of the algorithm is that the extension of each  $V_m^\lambda$  to a subspace supported on the full system would include a good approximation to the global low-energy eigenspace  $T$ . That is, each set  $V_m^\lambda$  is chosen such that if  $\mathfrak{H} = \mathfrak{H}_m^\lambda \otimes \bar{\mathfrak{H}}_m^\lambda$ , then  $V_m^\lambda \otimes \bar{\mathfrak{H}}_m^\lambda$  contains a subspace which is a good approximation to  $T$ . We identify a set  $V_m^\lambda$  to be  $\delta$ -viable if

$$P_T P_{V_m^\lambda \otimes \bar{\mathfrak{H}}_m^\lambda} P_T \geq (1 - \delta) P_T,$$

where  $P_S$  is a projector onto a subspace  $S$ . Consider the nondegenerate case, that is,  $T = \text{Span}(t)$ ,  $t \in \mathfrak{H}$ . Then the viability condition on  $V_m^\lambda$  leads to a definition of  $\delta$ :

$$\delta = 1 - \text{Tr} \left( P_{V_m^\lambda \otimes \bar{\mathfrak{H}}_m^\lambda} t t^\dagger \right). \quad (1)$$

For the case that  $\dim(T) > 1$ , maximize the above over all  $t \in T$ . The goal of the algorithm is to construct the viable sets in such a way that they are indeed  $\delta$ -viable for some small constant  $\delta$ . We emphasize that this viability condition is never explicitly checked, or formally guaranteed, by the algorithm.

If  $n$  is chosen to be small enough, generic operators on  $\mathfrak{H}_0^\lambda$  can be exactly diagonalized. In the initialization step, the initial viable set  $V_0^\lambda$  is specified to be the span of the  $s$  eigenvectors of  $H_0^\lambda$  of lowest energy, obtained by exact diagonalization.

### C. Iteration over scale

The algorithm proceeds through a tree-like hierarchy, the levels of which are specified by a scale parameter  $m = 0, 1, \dots, \log_2(N/n)$ . At scale  $m$ , block  $J_m^\lambda$  consists of  $2^m n$  sites and the region index  $\lambda$  runs from 0 to  $N/(2^m n) - 1$ . Note that although the scale of the algorithm is increasing, we do not eliminate any of the physical degrees of freedom. At each step we assume that the

The input is a local Hamiltonian  $H$  acting on  $N$  qubits, specified by an MPO. Let  $n$ ,  $s$  and  $D$  be input parameters.

1. Initialization:

- (a) Construct approximate ground state projector (AGSP)  $K$  from Hamiltonian  $H$
- (b) Partition system into contiguous blocks of length  $n$ , denoted  $J_0^\lambda$ ,  $\lambda = 0, 1, \dots, N/n - 1$ . Obtain  $s$ -dimensional low-energy eigenspace  $V_0^\lambda$  of block Hamiltonian  $H_0^\lambda$  for each  $\lambda$ .

2. For  $m = 0, 1, \dots, \log_2(N/n) - 1$ , denoting an “RG step” or scale factor:

- (a) Expansion: for  $\lambda = 0, 1, \dots, N/(2^m n) - 1$ :
  - i. Extract  $D^2$  operators  $\{A_{m,r}^\lambda\}_{r=1,\dots,D^2}$  from the AGSP  $K$ , acting on subsystem  $J_m^\lambda$ . Operate on the viable set, taking  $V_m^\lambda \rightarrow W_m^\lambda \equiv \{A_{m,r}^\lambda V_m^\lambda\}_r$ , where  $\dim(W_m^\lambda) \leq sD^2$ .
  - ii. Compute the restriction of the block Hamiltonian  $H_m^\lambda$  to  $W_m^\lambda \subset \mathfrak{H}_m^\lambda$ .
- (b) Reduction: For  $\lambda = 0, 2, \dots, N/(2^m n) - 1$ :
  - i. (Merge) Obtain the tensor product space  $W_m^\lambda \otimes W_{m+1}^{\lambda+1} \subset \mathfrak{H}_{m+1}^{\lambda/2}$ , supported on qubits in  $J_{m+1}^{\lambda/2} = J_m^\lambda \cup J_{m+1}^{\lambda+1}$ . Compute the restriction of  $H_{m+1}^{\lambda/2}$  to the tensor product set.
  - ii. Obtain  $s$ -dimensional low-energy eigenspace of the restriction of  $H_{m+1}^{\lambda/2}$  to the tensor product space. Use the eigenstates as a basis for viable set  $V_{m+1}^{\lambda/2}$  in iteration  $m + 1$ .

3. At  $m = m^* = \log(N/n)$ , the viable set  $V_{m^*}^0$  is a candidate for the low-energy space  $T$  supported on the full system.

Figure 1. Outline of the implemented RRG algorithm.

previous level has produced a viable set  $V_m^\lambda$  with basis  $\{v_q\}_{q=1,\dots,s}$  represented by MPS, for every  $\lambda$ .

The algorithm performs two steps. The first step is the *expansion* of the viable set, which has the effect of improving the viability parameter  $\delta$ , specified in Eq. (1). This is accomplished using the AGSP constructed in the initialization step as follows. Let  $J_{m,L}^\lambda$  denote the qubits to the left of  $J_m^\lambda$ , and  $J_{m,R}^\lambda$  those to the right. (Generally  $J_m^\lambda$  has two boundaries with its complement  $J_{m,L}^\lambda \cup J_{m,R}^\lambda$ . The system-edge cases follow immediately.) Consider the MPO representation of the AGSP  $K$ , whose elementary tensors are collections of operators on the local Hilbert space, as an MPS. The Schmidt decomposition of  $K$  across the left boundary, separating  $J_{m,L}^\lambda$  from  $J_m^\lambda \cup J_{m,R}^\lambda$ , produces a virtual index of dimension  $\zeta$ :

$$K = \sum_{\alpha < \zeta} \sigma_\alpha L_\alpha M_\alpha.$$

The right Schmidt vectors  $M_\alpha$  are operators on  $J_m^\lambda \cup J_{m,R}^\lambda$ , each with a corresponding Schmidt coefficient. The Schmidt decomposition may then be obtained for each of the  $M_i$  across the boundary between  $J_m^\lambda$  and  $J_{m,R}^\lambda$ , producing a virtual index of dimension  $\xi$ . That is,

$$M_\alpha = \sum_{\beta < \xi} \nu_{\alpha\beta} A_{\alpha\beta} R_{\alpha\beta}$$

Each  $A_{\alpha\beta}$  is an operator on  $\mathfrak{H}_m^\lambda$ , with weight  $\gamma_{\alpha\beta} = \sigma_\alpha \nu_{\alpha\beta}$  in the expansion of  $K$ . For clarity we make the algorithm variables explicit:  $A_{m,\alpha\beta}^\lambda$ . Now let  $D > 0$  be another parameter of the algorithm. In order to increase the viability of the set  $V_m^\lambda$ , act on it with the  $D^2$  operators  $A_{m,r}^\lambda$ ,  $r = (\alpha, \beta)$ , having highest weight

$\gamma_r = \gamma_{\alpha\beta}$ . That is, take  $V_m^\lambda \rightarrow W_m^\lambda = \text{Span}(\{A_{m,r}^\lambda v_q\}_{r,q})$ , which we refer to as an *expanded viable set* with dimension bounded by  $sD^2$ .

One expects this operation to produce a set  $W_m^\lambda$  of better viability than  $V_m^\lambda$  because the  $A_{m,r}^\lambda$  operators together are meant to increase overlap with the global low-energy space  $T$ : this is the defining property of the AGSP. More precisely, let  $\{v_j\}$  be a collection of states in  $V_m^\lambda$  such that there exists  $\{\bar{v}_j\} \in \bar{\mathfrak{H}}_m^\lambda$  such that for some Schmidt coefficients  $a_j$ , the state  $x = \sum_j a_j v_j \otimes \bar{v}_j$  has good overlap with  $T$ . By construction,  $Kx$  has better overlap with  $T$  than  $x$ . Using the previous decomposition,

$$Kx = \sum_{\alpha,\beta,j} \gamma_{m,\alpha\beta}^\lambda a_j A_{m,\alpha\beta}^\lambda v_j \otimes \bar{A}_{m,\alpha\beta}^\lambda \bar{v}_j,$$

where  $\bar{A}_{m,\alpha\beta}^\lambda = L_{m,\alpha}^\lambda R_{m,\alpha\beta}^\lambda$ . If all operators  $A_{m,\alpha\beta}^\lambda$  were applied to  $V_m^\lambda$ , the resulting set would contain the collection of states  $\{A_{m,\alpha\beta}^\lambda v_j\}$ , which has improved viability. However, instead of applying all  $A_{m,\alpha\beta}^\lambda$ , which would lead to an unmanageable blow-up in the size of the viable set, we introduce an approximation by selecting the  $D^2$  operators  $A_{m,r}^\lambda$  of highest weight  $\gamma_r$  in order to obtain  $W_m^\lambda$ . There is no formal guarantee that this is the best choice, as the Schmidt decomposition is based on the Frobenius rather than operator norm. In practice we found the choice to be quite reasonable: to observe the increase in viability in a nondegenerate gapped model, compare the  $V$  and  $W$  points in Fig. 3, and in a critical model in Figs. 5, 6.

The second step performed at each scale  $m$  is that of *reduction* of the dimension of the expanded viable sets  $W_m^\lambda$  and  $W_{m+1}^{\lambda+1}$  to generate  $V_{m+1}^{\lambda/2}$ . At the cost of a loss of viability, this step restores  $s$ -dimensionality, resulting

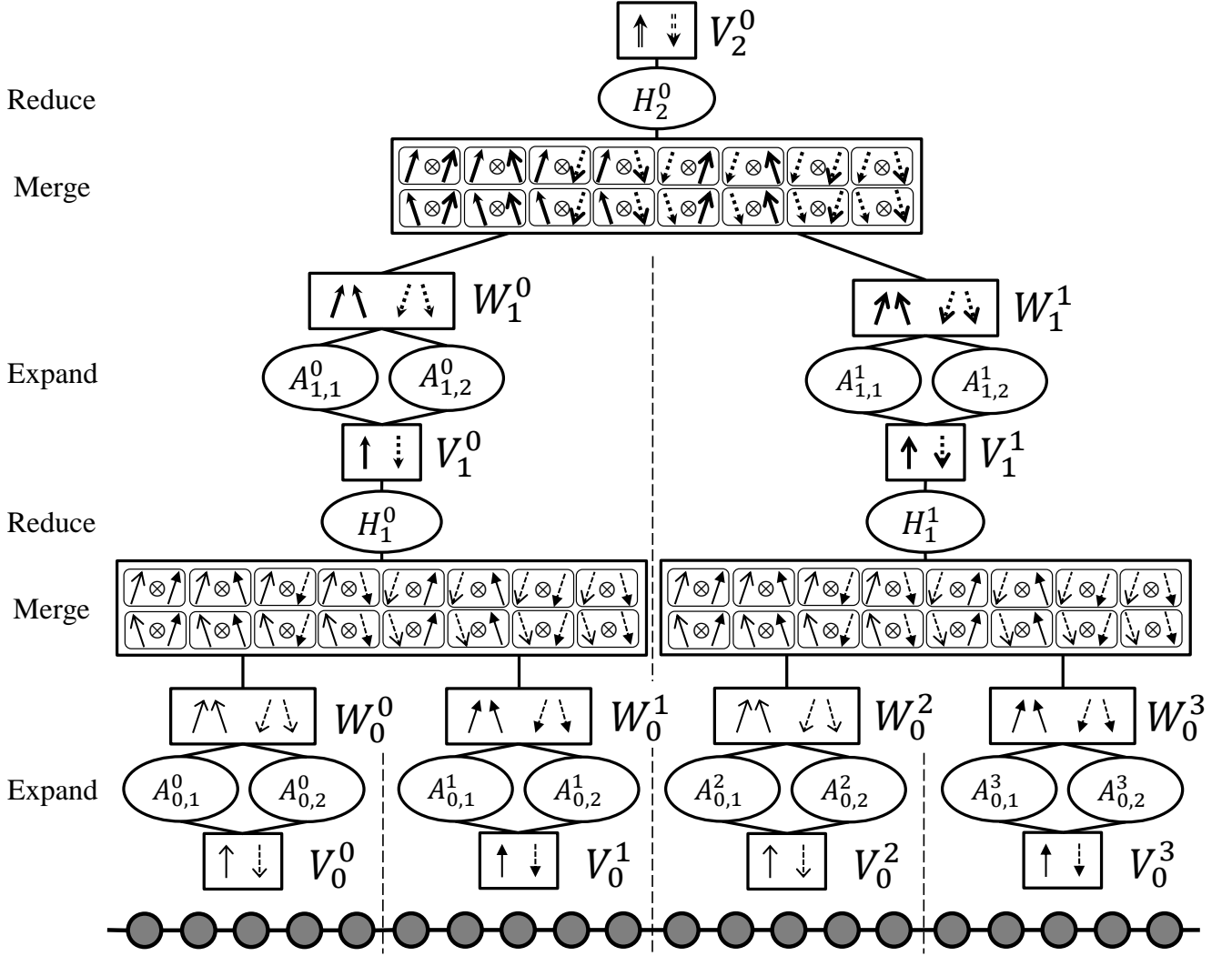


Figure 2. Illustration of the RRG algorithm operating over several length scales  $m = 0, 1, 2$ . The parameters shown are  $(s, D) = (2, 2)$ , and block size  $n = 5$ . The arrows represent vectors in Hilbert space, and the gray dots represent lattice sites.

in a viable set suitable to use at the next level. One first performs a *merge* operation on disjoint pairs of blocks  $(\lambda, \lambda+1)$ , with  $\lambda = 0, 2, \dots, N/(2^m n) - 2$ . Merging refers to computing the tensor product set  $W_m^\lambda \otimes W_{m+1}^{\lambda+1}$  that has support on sites  $J_m^\lambda \cup J_{m+1}^{\lambda+1}$ . One obtains the viable set  $V_{m+1}^{\lambda/2}$ , a subspace of  $\mathfrak{H}_{m+1}^{\lambda/2} = \mathfrak{H}_m^\lambda \otimes \mathfrak{H}_{m+1}^{\lambda+1}$ , from the  $s$ -dimensional low-energy eigenspace of the restriction of  $H_{m+1}^{\lambda/2}$  to  $W_m^\lambda \otimes W_{m+1}^{\lambda+1}$ . We note that this step differs from its counterpart in the theoretical algorithm, which proceeds via random sampling instead of deterministically selecting the lowest-energy eigenvectors of  $H_{m+1}^{\lambda/2}$ , as we do here. Our choice is based on efficiency considerations described below; see also Appendix A for further discussion. The effect of the operation on the viability of the reduced subspaces can be seen in Figs. 3, 5, and 6.

The single viable set  $V_{m^*}^0$  generated at  $m^* = \log_2(N/n)$  after the reduction step at scale  $m^* - 1$ , is a constant-dimensional  $\delta$ -viable subspace with support on the full

system. The algorithm returns the  $s$  lowest-energy eigenvectors of the restriction of  $H$  to  $W_{m^*-1}^0 \otimes W_{m^*}^1$ , which comprise a basis for this candidate subspace.

#### D. Scaling and computational considerations

The accuracy with which RRG approximates low-energy eigenstates of  $H$  is controlled primarily by two parameters,  $s$  and  $D$ . To recapitulate,  $s$  bounds the dimension of the reduced viable sets at each step, and  $D$  controls the level of approximation in the application of the AGSP via the operators  $\{A_{m,r}^\lambda\}$ ,  $r = 1, \dots, D^2$ . Both parameters are reflected in the bound on the dimension  $sD^2$  of the expanded viable sets  $W_m^\lambda$ .

We review the steps in the algorithm and discuss their complexity scaling based on these parameters. In addition to  $s$  and  $D$ , important parameters are the system size

$N$  and the bond dimensions  $\chi$  for MPS and  $\eta$  for MPO that are manipulated throughout. For physical Hamiltonians it is reasonable to expect  $\chi$  and  $\eta$  to be constant in the gapped case, and in gapless systems  $\chi, \eta \sim N$ . See Schollwöck<sup>4</sup> for a discussion of the scaling of basic MPS operations.

The initialization requires obtaining viable sets  $V_0^\lambda$  of the Hilbert space  $\mathfrak{H}_0^\lambda$  on the qubits  $J_0^\lambda$ . For small enough choices of  $n$  the complexity of this step will be negligible, so we omit it. Similarly, the computation of the full AGSP  $K \approx (e^{-H/t})^k$  can be done efficiently via Trotter decomposition, and is not an important bottleneck.

For the steps comprising the iterated procedure we give scaling results applicable at the final computational level  $m = m^* - 1$ . The first step is to apply  $K$  to each  $V_m^\lambda$  by means of the Schmidt decomposition of  $K$  across the boundary separating  $J_m^\lambda$  from its complement  $\bigcup_{\lambda' \neq \lambda} J_m^{\lambda'}$ . This yields a set of operators acting on  $\mathfrak{H}_m^\lambda$ . Applying the  $D^2$  such operators of highest Schmidt weight to a basis of the subspace takes  $V_m^\lambda \rightarrow W_m^\lambda$ , increasing the dimension to  $sD^2$ . The total cost of contracting these MPS and MPO is  $\mathcal{O}(sD^2N\chi^2\eta^2)$ .

The second step acts on disjoint pairs of neighboring regions, forming the tensor product of expanded viable sets:  $W_m^\lambda \otimes W_m^{\lambda+1}$ , with dimension  $(sD^2)^2$ . We compute the matrix elements of the restriction of the block Hamiltonian to the tensor product set. The scaling of this step is  $\mathcal{O}([(sD^2)^2]^2N\chi^3)$ . For local Hamiltonians the constant can be improved using the decomposition

$$\begin{aligned} H_{m+1}^{\lambda/2} &= H_m^\lambda + H_m^{\lambda+1} + B_{m+1}^{\lambda/2} \\ &= H_m^\lambda + H_m^{\lambda+1} + \sum_p B_{m,p}^\lambda \otimes B_{m,p}^{\lambda+1}. \end{aligned}$$

The operator  $B_{m+1}^{\lambda/2}$  contains  $\mathcal{O}(1)$  terms in  $H$  acting across the boundary between  $J_m^\lambda$  and  $J_m^{\lambda+1}$ .

Exact diagonalization of the restricted block Hamiltonian in the subspace has complexity  $\mathcal{O}([(sD^2)^2]^3) = \mathcal{O}(s^6D^{12})$ . After this, the final step is to explicitly compute the  $s$  lowest-energy eigenstates, which has a total cost  $\mathcal{O}(s(sD^2)^2N\chi^3)$ . These states are used as a basis for the viable set at the next iteration.

From this coarse analysis it is clear that the limiting step with respect to  $s$  and  $D$  is the diagonalization of the restricted block Hamiltonian. This step is not part of the original formulation, which specifies instead that the reduction of viable set dimension take place by randomly selecting states from the tensor product set. The choice of our variant is motivated by its effect on the entanglement of the intermediate basis states: low-energy excited states of a block Hamiltonian may display lower entanglement than states chosen randomly. In practice this lowers  $\chi$  in some systems. It also demonstrates a different possible interpretation of the parameter  $s$ , which during the iteration step implicitly defines an energy scale with respect to the restricted Hamiltonian. States having block excitation energy higher than this scale are inaccessible to the algorithm for the purposes of the expansion step.

### III. NUMERICAL RESULTS

We now present results from RRG for some example models with the following goals in mind. We first validate the algorithm in a simple gapped nondegenerate system in Sec. III A, demonstrating consistency with DMRG output as well as previous numerical and perturbation theory results. In this case the states obtained by RRG are of similar accuracy to those of DMRG, with run times a factor of 5–10 slower depending on  $s$ ,  $D$ , and  $N$ . However, we emphasize that it is not the objective of RRG to obtain a numerically precise ground state; rather, it is to accurately identify the global low-energy subspace. One expects an optimization algorithm to obtain a more precise state in the absence of local energy minima, and we generally take the DMRG ground state to be exact (in particular, using it to measure viability  $\delta$ ). The RRG candidate states may later be variationally optimized in order to achieve a particular accuracy. We expect that this procedure would be very fast, but we do not modify the candidate states here.

Our next goal is to demonstrate the practical scaling of the algorithm's performance and computational costs associated with the subspace parameters  $(s, D)$ . We use the familiar case of the Ising model in the transverse field in Sec. III B, both away from and at criticality. We find that for low values of these parameters, often surprisingly good results can be obtained, with close to unity overlap between DMRG and RRG ground state candidates. However, neither algorithm scales linearly with system size in the critical regime. Here the slowdown of RRG is no longer a simple numerical factor but becomes a significant cost at larger system sizes (beyond a few hundred sites in our implementation) or for larger values of the algorithm parameters.

Finally, we consider somewhat more challenging models demonstrating areas in which RRG may hold an advantage. In Sec. III C we investigate the Bravyi-Gosset model,<sup>19</sup> which has  $\mathcal{O}(N)$  ground state degeneracy, by obtaining a complete basis for the ground space. In Sec. III D we consider the XY model with randomly-distributed couplings. The ground state of this model, the random singlet phase, displays long-range entanglement in that it supports algebraic decay of correlations. We compare the correlations present in the candidate states of DMRG and RRG to exact results obtained by the Jordan-Wigner transformation, finding that RRG more accurately reproduces observables measured on the state.

All numerical results were obtained using the tensor network library ITensor<sup>20</sup> for both the DMRG and RRG computations. In all of the following, a Trotter decomposition with 60 steps was used to obtain the tensor network for  $Q_t \approx e^{-H/t}$ , with  $t = 10$ , and degree  $k = 8$  used to compute the AGSP  $K \approx (Q_t)^k$ . Thus the effective temperature  $t/k$  is of order unity. The trials were run on standard hardware on a single node of a computing cluster with single threading only for the reported run

times. A single error parameter  $\tau$  was used to control MPS truncation in ITensor for both DMRG and RRG (usually  $\tau \sim 10^{-9}$ – $10^{-12}$ ); in most cases a more lenient value would drastically improve run times with little effect on accuracy. DMRG convergence was handled using a fixed number of sweeps  $\geq 20$ . Excited states were found iteratively in DMRG using random trial wavefunctions. Often the average viability will be used as a metric; this is simply the average over region label  $\lambda$  of the viability, as defined in Eq. (1), of each viable set ( $V_m^\lambda$  or  $W_m^\lambda$ ) at fixed level  $m$ .

### A. Nonintegrable Ising model

This model refers to a spin-1/2 Hamiltonian

$$H = -J \sum_{i=0}^{N-2} \sigma_i^z \sigma_{i+1}^z - g \sum_{i=0}^{N-1} \sigma_i^x - h \sum_{i=0}^{N-1} \sigma_i^z.$$

For  $h \neq 0$  the model is gapped with a nondegenerate ground state, and admits no good quantum numbers due to the longitudinal component of the field. A recent numerical study<sup>21</sup> for the parameters  $(J, g, h) = (1, -1.05, 0.5)$  found the ground state energy density to be  $\varepsilon_0/N \approx -1.722$  and the gap  $\gamma = 3.6401$ .

We run the RRG algorithm for a fixed system size  $N = 256$ , initial block size  $n = 8$ , and track the average viability  $\delta$  of the viable sets  $V_m$  and  $W_m$  through the sequence of dimensional expansion and reduction at each scale  $m$  (see Fig. 2). Each data point shown in Fig. 3 is the average over  $\lambda$  at a given length scale  $m$ . The parameters  $(s, D)$  are varied to demonstrate their influence on the results. Because the model is gapped, the AGSP is an effective projector even at low values of  $D$ . Consequently, the accuracy of RRG for the largest  $(s, D)$  is comparable to that of DMRG. We do not expect this to be a general feature. For gapped systems of this size both DMRG and RRG have run times scaling linearly with system size, however RRG runs more slowly by a factor of 5–10 compared to DMRG. At  $N = 256$ , DMRG took 5 minutes to converge  $s = 5$  states (ground and four excited) and RRG ran in 30 minutes with  $(s, D) = (5, 3)$ .

The final  $s$ -dimensional viable sets  $V_{m^*}$  ( $V_5$  in Fig. 3) here and in the following examples display much better average viability than that of the previous  $V_m$ . This is generally true: at steps  $m < m^*$  the viable set is obtained by diagonalizing a restricted block Hamiltonian  $H_m^\lambda$ , which omits terms present in  $H$ . The low-energy eigenspace of this operator need not be close to  $T$ , the global low-energy space. At  $m = m^*$ , however, the low-energy eigenspace of  $H_{m^*}^0 = H$  coincides with  $T$ , resulting in minimal loss of viability from the dimensional reduction.

By changing the parameters of RRG, we are also able to obtain candidates for low-energy excited states. The ground state of this model is close to a uniform spin-up

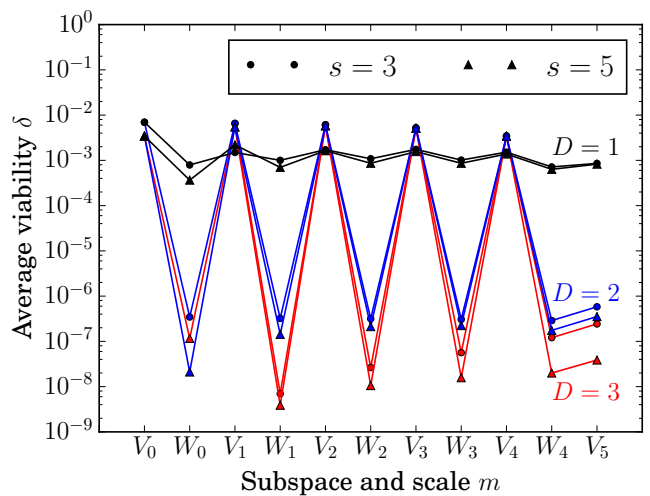


Figure 3. (color online) Viability of sets  $V_m^\lambda$ ,  $W_m^\lambda$  averaged over  $\lambda$ , for nonintegrable Ising model with  $N = 256$  spins, obtained as the RRG algorithm progresses through the scale hierarchy. Data are shown for parameter values  $s = 3, 5$  and  $D = 1, 2, 3$ .

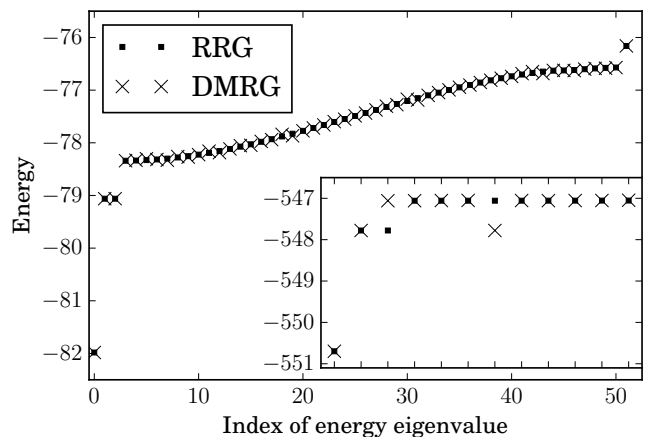


Figure 4. Energy eigenvalues of the nonintegrable Ising Hamiltonian for  $N = 48$  within the subspace obtained by RRG for  $(s, D) = (52, 3)$ , along with DMRG results for low-energy states. Inset: the same computation for  $N = 320$  and  $(s, D) = (12, 3)$ . DMRG does not consistently identify both edge states in sequence; see text for details.

state, and the first excited band contains a spin-flip excitation. Under open boundary conditions two nearly degenerate lower-energy states separate from the first band, corresponding to quasiparticles localized at either edge. We obtain the low-energy spectrum for  $N = 48$  with  $(s, D) = (52, 3)$ , and for  $N = 320$  with  $(s, D) = (12, 3)$ . The results are shown in Fig. 4, compared with DMRG states. For small  $N$  both methods find the entire first excited band. In the larger system, the localized edge states are somewhat more difficult for DMRG to obtain, and it does not consistently find the edge states in sequence. The computed RRG ground state energy den-

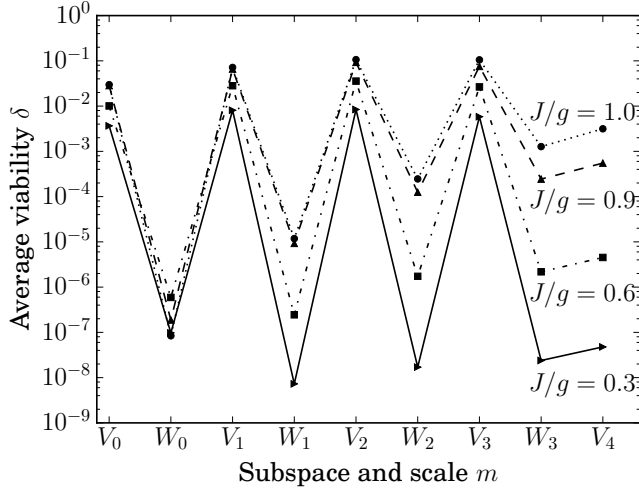


Figure 5. Viability of sets  $V_m^\lambda, W_m^\lambda$ , averaged over  $\lambda$ , for the transverse-field Ising model both away from and at criticality. The number of spins is  $N = 128$ . All data points were generated using parameter values  $(s, D) = (5, 4)$ .

sity at  $N = 320$  is  $\varepsilon_0/N = -1.721$  and the gap to the excited band is  $\gamma = 3.6402$ , in agreement with previous results. We find the half-chain entanglement entropy of the ground state and edge states to be  $S = 0.01$  bits, and of the states in the band to be  $S \approx 1.01$  bits, consistent with qualitative understanding of these states.

### B. Transverse-field Ising model

Consider the same Hamiltonian in the regime  $h = 0$ ; that is, the Ising model in a transverse field. Fig. 5 shows the result as we approach the critical point  $J = g$  from the paramagnetic phase for  $N = 128$ , measuring average viability throughout the algorithm. One observes a strong deterioration of the final viability as the gap closes. Approaching the critical point, RRG takes increasingly more time than DMRG to run: in these trials for  $J/g = 0.6$  DMRG takes 400 seconds and RRG takes 5000 seconds, but for  $J/g = 1.0$  DMRG takes 800 seconds and RRG takes 22000 seconds.

We also demonstrate the scaling with parameters  $s$  and  $D$  at the critical point in Fig. 6. The improvement on viability with increasing  $D$  is more systematic and less dramatic than seen in Fig. 3, corresponding to a relatively flat spectrum of Schmidt values across the cuts made between subsystems. As the algorithm progresses, viability visibly decreases, in contrast to the previous gapped case, which maintains a consistent viability throughout.

### C. Bravyi-Gosset model

This model was initially introduced as a classification scheme for frustration-free 2-local Hamiltonians.<sup>19</sup> The

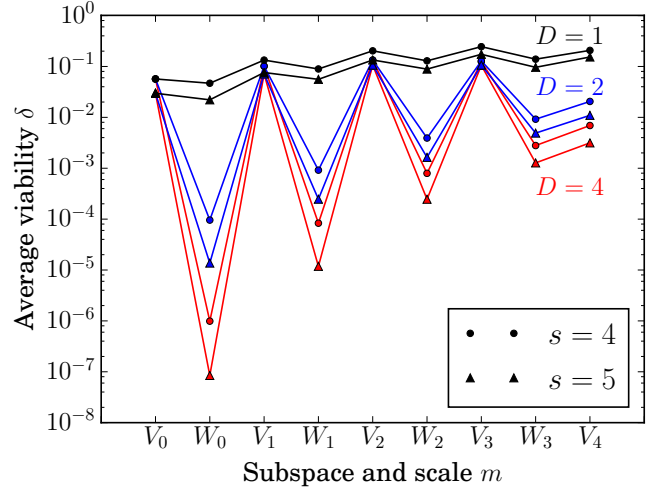


Figure 6. (color online) Viability of sets  $V_m^\lambda, W_m^\lambda$ , averaged over  $\lambda$ , for the transverse-field Ising model at criticality, obtained as the RRG algorithm progresses through the scale hierarchy. Data are shown for parameter values  $s = 4, 5$  and  $D = 1, 2, 4$ .

Hamiltonian is

$$H = \sum_{i=0}^{N-2} |\psi\rangle\langle\psi|_{i,i+1}, \quad (2)$$

where  $|\psi\rangle$  is a generic state on two qubits. Up to a global phase, such a state can be specified as  $|\psi\rangle = R(\theta)_1 (p|00\rangle + \sqrt{1-p^2}|11\rangle)$ , with  $R(\theta)_1$  a rotation performed on the first qubit. As the spectrum is invariant under global rotation, the Hamiltonian is fully specified by the two parameters  $\theta \in [0, 2\pi)$ ,  $p \in [0, 1/2]$ . Restricting to  $\theta = 0$ , we may rewrite Eq. (2) in a more familiar notation:

$$H = \sum_{i=0}^{N-2} \left( \frac{\sqrt{p(1-p)}}{2} (\sigma_i^x \sigma_{i+1}^x - \sigma_i^y \sigma_{i+1}^y) + \frac{1}{4} \sigma_i^z \sigma_{i+1}^z \right) + \sum_{i=0}^{N-1} \left( \frac{1-2p}{4} \sigma_i^z + \frac{1}{8} \right)$$

That is, this model is equivalent to a particular anisotropic Heisenberg model in a fine-tuned field. For any value of  $p$  the system exhibits  $(N+1)$ -fold ground state degeneracy. Basis states for the ground space can roughly be thought of as having two regions of differing magnetization, with an interface which can be located at any site with ground state energy  $\varepsilon_0 = 0$ . (Refer to Bravyi and Gosset<sup>19</sup> for a full description.) Therefore the algorithm choice  $s \geq N+1$  is sufficient to obtain the full ground space.

The low-energy spectrum obtained by RRG for this model at  $N = 32$  is shown in Fig. 7, along with the DMRG results. We use  $p = 1/2$ ; that is,  $|\psi\rangle$  is a Bell state. Using  $(s, D) = (36, 3)$ , RRG identifies the full



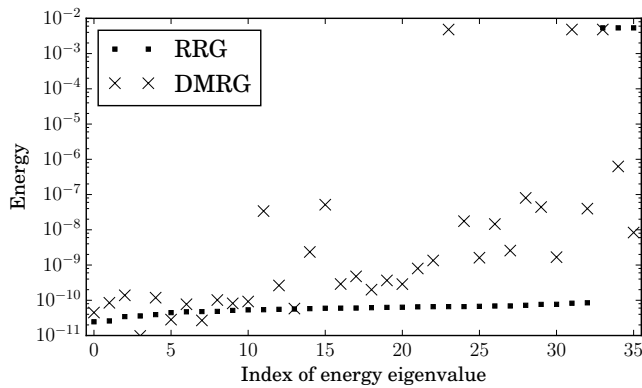


Figure 7. Energy eigenvalues of Bravyi-Gosset model with  $N = 32$  sites within the subspace obtained by RRG for  $(s, D) = (36, 3)$ . Also shown are DMRG results for the 36 lowest-energy states.

zero-energy ground space to within an accuracy determined by  $\tau$ , the truncation error of the MPS. In contrast, obtaining the full ground space of this model is challenging for DMRG, which becomes hampered by candidate states of very high entanglement, often requiring a bond dimension an order of magnitude larger than those of RRG candidate states in order to achieve similar truncation error. These not only are computationally intensive to optimize, but also present DMRG with difficulty finding further excited states, as the modified Hamiltonian includes nonlocal projectors. Thus, the candidate states are not accurate eigenstates of the original Hamiltonian. This difficulty is evident in run times as well; to obtain the data shown took 10 hours for RRG and 40 hours for DMRG. For the latter, use of a specialized approach like multiple targeting could improve accuracy, or diagonalization of the original Hamiltonian within the subspace spanned by the DMRG candidate states could recover much of the ground space; however, no such specialized approach is needed for RRG.

#### D. Random XY model

The random XY model is an inhomogeneous spin-1/2 system with Hamiltonian

$$H = \sum_{i=0}^{N-2} J_i (\sigma_i^x \sigma_{i+1}^x + \sigma_i^y \sigma_{i+1}^y),$$

where the position-dependent coupling constants  $J_i$  are drawn from a random distribution. If the logarithm of the distribution is broad, Dasgupta-Ma real-space renormalization group analysis identifies the ground state as the random singlet phase, in which pairs of spins form singlet states at all length scales.<sup>22–25</sup> This model is tractable by the Jordan-Wigner transformation, which maps onto free spinless fermions. We use this system as

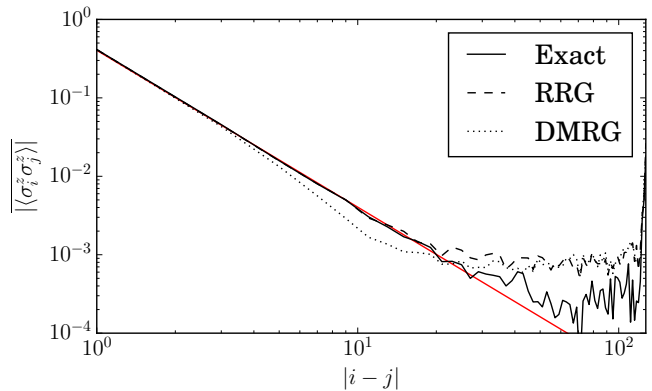


Figure 8. (color online) Disorder-averaged decay of correlations of candidate ground states of the random XY model for  $N = 128$ , as compared to exact results obtained through the Jordan-Wigner transformation. The predicted power-law behavior is indicated by the red line.

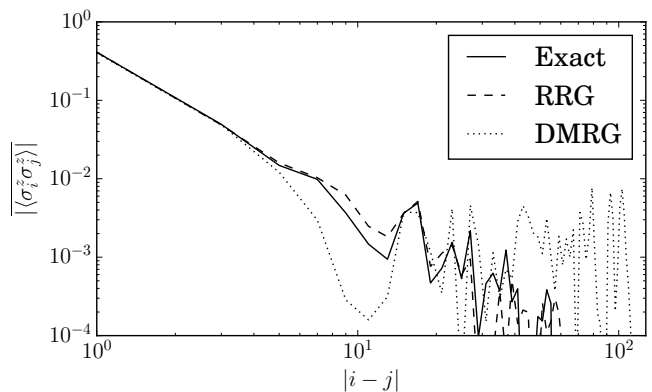


Figure 9. A typical “hard” instance contained in the disorder average above, with energy gap  $\gamma \approx 10^{-7}$ . This is sufficiently large for RRG to track the long-range correlations with  $(s, D) = (4, 5)$ . DMRG displays a tendency for lower correlations until saturating at the noise floor.

a benchmark of algorithmic ability to encode long-range correlations in the ground state.

We use the following distribution for the Hamiltonian terms:  $p(J_i) = \frac{1}{\Gamma} J_i^{-(1+\frac{1}{\Gamma})}$ ,  $J_i \in (0, 1]$ , with  $\Gamma$  controlling the width of the distribution of log-energies.<sup>25</sup> We fix  $\Gamma = 2$ , which is sufficiently broad that the ground state is composed predominantly of localized singlet states on neighboring sites, along with spatially separated correlated qubits occurring at all length scales. As a metric we use the average two-point correlation function  $\langle \sigma_i^z \sigma_j^z \rangle$  as a function of separation  $r = |i - j|$  in the ground state, which is known to decay algebraically as  $r^{-2}$ . This quantity is compared to exact diagonalization results from the inhomogeneous free fermion description in Fig. 8.

These results are intended to present a fair comparison between DMRG and RRG. Both methods used unrestricted MPS bond dimension to achieve a truncation



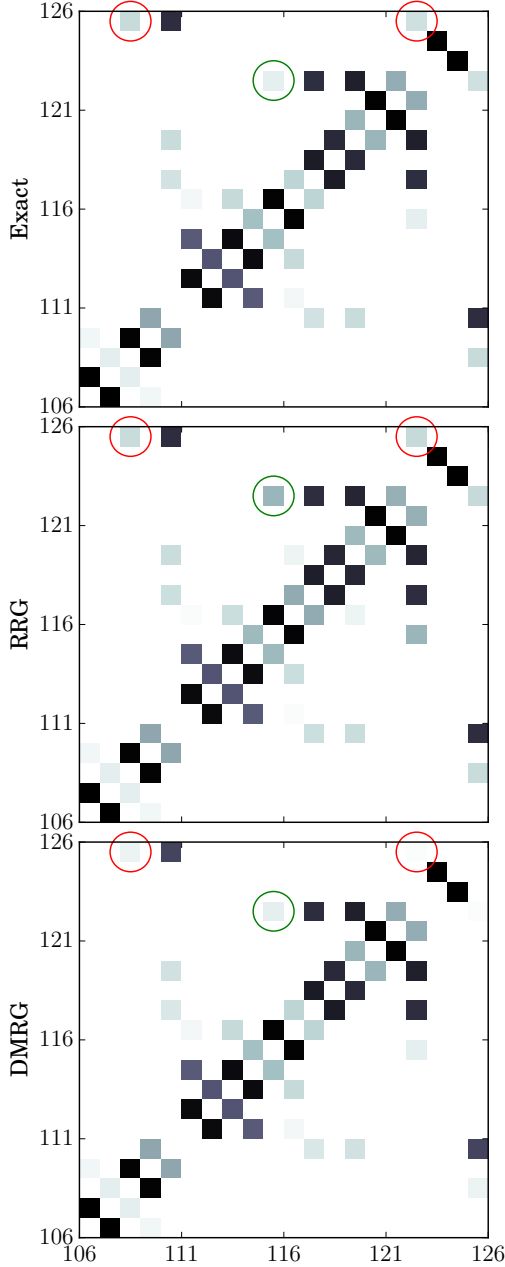


Figure 10. (color online) Expectation value  $\langle \sigma_i^z \sigma_j^z \rangle$ , where sites  $i$  and  $j$  are given by the axes for  $i, j \in [106, 125]$ . The color scales with  $\log |\langle \sigma_i^z \sigma_j^z \rangle|$  and runs from  $[-2, 0]$  in all plots, with darker color indicating a higher value. The diagonal is omitted. Circles mark particular sites where differences between exact results and candidate states are evident. This disorder realization is the same “hard” instance shown in Fig. 9.

error  $\tau \leq 10^{-12}$ . Typically the ground state bond dimension is similar for both methods. The RRG parameters are  $(s, D) = (4, 5)$ . DMRG used 20 sweeps per state, and convergence of several “hard” examples (see below) was confirmed using 50 sweeps. DMRG typically took 1 hour to converge  $s = 4$  states and RRG took 8 hours to complete. The average is over 150 disorder realizations.

The observed “saturation” of the correlations of Fig. 8 to a noise floor arises from the structure of the low-energy excited states. For a broad initial distribution, the energy gap of a specific disorder Hamiltonian may be very small. For any method using MPS, a lower limit on the gap in order to distinguish the ground state (at energy  $\varepsilon_0$ ) is  $\gamma \sim \tau \varepsilon_0$ , below which the MPS truncation procedure will randomly select a vector from the low-lying subspace. However, even for realizations with much larger gaps a candidate ground state may include substantial contributions from low-energy excited states. A singlet of length  $l$  has energy scale  $\varepsilon \sim e^{-\sqrt{l}}$ ; thus, the low-lying states involve excitations localized on the long-range entangled sites. Choosing a random superposition of these amounts to white noise at long distances. Instances of such Hamiltonians in the disorder average must necessarily eventually overwhelm the decay of correlations; here the distribution of energy gaps is very broad on a log scale,<sup>26</sup> so these cases are frequent.

For disorder-averaged correlations at short range up to  $|i - j| \approx 20$ , RRG reproduces algebraic decay of correlations matching the exact results. In contrast, the DMRG candidate states demonstrate stronger decay of correlations. There is no systematic difference in MPS bond dimension between DMRG and RRG, indicating that RRG is not simply using additional resources, but is indeed more sensitive to long-range correlations.

Independent of the saturation due to the energy gap, the disorder average comprises both “easy” and “hard” instances. In easy cases both DMRG and RRG match the exact results closely at all length scales. In the hard cases both algorithms obtain the correlations only approximately, but DMRG appears to consistently underestimate correlations. RRG does not demonstrate a tendency towards either enhanced or reduced correlations. We provide an example of the spatially averaged correlations from a hard disorder realization in Fig. 9. Fig. 10 shows an example of measured correlations  $\langle \sigma_i^z \sigma_j^z \rangle$  for various sites  $i, j \in [106, 125]$  in this particular disorder realization. Each square corresponds to a measurement  $\langle \sigma_i^z \sigma_j^z \rangle$  where  $(i, j)$  are specified by the axes. Darker squares indicate a larger magnitude of correlation between these sites. We show the exact results, RRG, and DMRG, and indicate some particular pairs of sites where either DMRG (red) or RRG (green) differ visibly from exact results. These variations in certain entangled sites tend toward reduced correlations in DMRG candidate ground states; it is unclear how much additional sweeping is required to compensate. RRG shows similar inaccuracies, but these are random, due to states missing from certain viable sets. Accurate correlations emerge in the disorder-averaged value, and the performance on individual disorder realizations can be controllably improved by tuning the dimension of the viable sets through the parameters  $s$  and  $D$ .

#### IV. DISCUSSION

DMRG has long been the method of choice for almost any numerical calculation involving ground states of 1D systems, and over time both its efficiency and range of applicability have gone through multiple improvements and extensions. One of the main findings of our initial numerical investigation is that the RRG algorithm, developed purely for theoretical purposes, can in fact be made quite effective in practice, to the point of providing a potentially viable alternative to DMRG in cases of practical interest. We stress that the choices of parameters that we employ in our numerics are quite far from the theoretically guaranteed regime, in order that the algorithm can be feasibly run. Additionally, many of the building blocks required for the theoretical proof have been altered in our implementation. Therefore the strict theoretical guarantees no longer hold. Regardless, we find that RRG obtains ground state candidates having large overlap with the true ground state in a variety of physically relevant models, and surpasses existing techniques in obtaining low-energy excited states and ground states of particular models demonstrating large degeneracy or long-range entanglement.

At present the run times required by the algorithm remain a challenge. Thus, the feasibility of RRG as a numerical method is essentially determined by the scaling discussed previously. This situation does invite future improvements. Some are immediate: for example, one may exploit symmetries of a particular problem (say, reflection symmetry across the middle of the system) in order to reduce duplication of work. Other improvements to the current implementation are more technical. For example, as described here the management of subspaces is clumsy: operations such as addition of MPS necessitate keeping careful track of gauge and add computational overhead for what is in principle a simple procedure. The use of data structures more appropriate to these operations could ameliorate scaling problems in all steps of the algorithm.

Indeed, an advantage of RRG is precisely this flexibility, to operate independently of a specific representation of states in Hilbert space. Here we have described an MPS RRG. In order to translate the logic to subspaces whose basis states are described by MERA—as would be natural for critical phases—one needs only the ability to perform evaluation of observables and addition. The former is a standard contraction which is highly efficient in MERA, and the latter can be seen as a variational process on overlaps, providing a straightforward interpretation as

a MERA operation. Other tensor network ansätze may also be amenable: with regard to PEPS, RRG could constitute a natural framework for solving models in higher dimensions, as the hierarchical structure generalizes in an evident way. Systems with periodic boundary conditions also present an interesting generalization, as until the final level the steps of the algorithm are insensitive to the system boundaries, provided an appropriate AGSP is given.

Our numerical results suggest situations in which RRG may perform well relative to existing algorithms. The first, informed by Sec. III A, is a case in which localized and delocalized excitations lie close in energy. An optimization algorithm operating on local degrees of freedom in a sweeping pattern may exhibit a bias towards delocalized excitations, which allow for effective optimization on many lattice sites. RRG is largely insensitive to such distinctions. The second case is that of Sec. III C, exhibiting highly degenerate ground states. The full ground space is more accurately found in its entirety by RRG than DMRG. The iterative DMRG procedure of finding states is susceptible to finding poor or highly entangled candidates, which reduce the accuracy of subsequent candidates. Such a limitation is not fundamental and could likely be eliminated by modification of the procedure; however no such modification is necessary for RRG. Finally, in Sec. III D we observe in the random XY model in the random singlet phase that long-range correlations are encoded more precisely in the ground state candidate of RRG than of DMRG, influencing observables computed for the state.

The examples we provide illustrate specific properties indicating that a model may be well suited for RRG. However, very little is known about its more general performance: other systems with disorder, periodic boundary conditions, and higher dimensions all pose interesting challenges and could constitute exciting new directions within this formalism.

#### ACKNOWLEDGMENTS

We acknowledge useful discussions with M. Fishman and S. White’s research group, as well as with C. White and C.-J. Lin. The numerical results were computed with the ITensor library<sup>20</sup> of E. Stoudenmire and S. White. This work was supported by the Institute for Quantum Information and Matter, an NSF Physics Frontiers Center, with support of the Gordon and Betty Moore Foundation. Additional funding support was provided by the NSF through Grant DMR-1619696.

---

\* broberts@caltech.edu

<sup>1</sup> I. Arad, Z. Landau, U. Vazirani, and T. Vidick, “Rigorous RG algorithms and area laws for low energy eigenstates in 1D,” (2016), arXiv:1602.08828.

<sup>2</sup> S. R. White, Phys. Rev. Lett. **69**, 2863 (1992).

<sup>3</sup> F. Verstraete, V. Murg, and J. Cirac, Advances in Physics **57**, 143 (2008).

<sup>4</sup> U. Schollwöck, Annals of Physics **326**, 96 (2011).

- <sup>5</sup> K. G. Wilson, Rev. Mod. Phys. **47**, 773 (1975).
- <sup>6</sup> S. R. White, R. M. Noack, and D. J. Scalapino, Phys. Rev. Lett. **73**, 886 (1994).
- <sup>7</sup> X. Chen, Z.-C. Gu, and X.-G. Wen, Physical Review B **83**, 035107 (2011).
- <sup>8</sup> M. Levin and C. P. Nave, Phys. Rev. Lett. **99**, 120601 (2007).
- <sup>9</sup> Z.-C. Gu, M. Levin, and X.-G. Wen, Phys. Rev. B **78**, 205116 (2008).
- <sup>10</sup> G. Evenbly and G. Vidal, Phys. Rev. Lett. **115**, 180405 (2015).
- <sup>11</sup> G. Vidal, Physical Review Letters **99**, 220405 (2007).
- <sup>12</sup> G. Evenbly and G. Vidal, Physical Review B **79**, 144108 (2009).
- <sup>13</sup> R. N. Pfeifer, G. Evenbly, and G. Vidal, Physical Review A **79**, 040301 (2009).
- <sup>14</sup> G. Evenbly and G. Vidal, Phys. Rev. B **81**, 235102 (2010).
- <sup>15</sup> G. Evenbly and G. Vidal, Phys. Rev. Lett. **115**, 200401 (2015).
- <sup>16</sup> Z. Landau, U. Vazirani, and T. Vidick, Nature Physics **11**, 566 (2015).
- <sup>17</sup> I. Arad, Z. Landau, and U. Vazirani, Phys. Rev. B **85**, 195145 (2012).
- <sup>18</sup> M. Suzuki, Progress of theoretical physics **56**, 1454 (1976).
- <sup>19</sup> S. Bravyi and D. Gosset, Journal of Mathematical Physics **56**, 061902 (2015).
- <sup>20</sup> E. M. Stoudenmire and S. R. White, "ITensor - Intelligent Tensor Library," <http://itensor.org>.
- <sup>21</sup> C.-J. Lin and O. I. Motrunich, Phys. Rev. A **95**, 023621 (2017).
- <sup>22</sup> R. N. Bhatt and P. A. Lee, Phys. Rev. Lett. **48**, 344 (1982).
- <sup>23</sup> S.-k. Ma, C. Dasgupta, and C.-k. Hu, Phys. Rev. Lett. **43**, 1434 (1979).
- <sup>24</sup> C. Dasgupta and S.-k. Ma, Phys. Rev. B **22**, 1305 (1980).
- <sup>25</sup> D. S. Fisher, Phys. Rev. B **50**, 3799 (1994).
- <sup>26</sup> D. S. Fisher and A. P. Young, Phys. Rev. B **58**, 9131 (1998).

## Appendix A: Differences from Arad *et al.*<sup>1</sup>

In this appendix we give a detailed account of the main points of departure of our numerical procedure from the theoretically guaranteed algorithm introduced in Arad *et al.*<sup>1</sup>, giving heuristic justification for our choices. We refer to the paper for a more thorough introduction to the main concepts discussed here, such as the notion of viable set and AGSP.

For concreteness we base our comparison on the algorithm presented in Arad *et al.*<sup>1</sup> for the case of a local Hamiltonian with degenerate gapped ground space (Assumption (DG)). The algorithm is stated as Algorithm 1 in Arad *et al.*<sup>1</sup>. It consists of two main steps, *Generate* and *Merge*. The two steps together recursively construct a sequence of viable sets  $V_m^\lambda$  for an  $N$ -qubit local Hamiltonian, where as in the main text  $m$  denotes a scale parameter and  $\lambda$  indexes a subregion.

### 1. Generate

The goal of the *Generate* step is to generate an MPO representation for a suitable AGSP. In Arad *et al.*<sup>1</sup> a fresh AGSP is computed for each scale  $m$  and region  $\lambda$ . Given a decomposition  $\mathfrak{H} = \mathfrak{H}_L \otimes \mathfrak{H}_m^\lambda \otimes \mathfrak{H}_R$ , a global AGSP is defined as  $K_m^\lambda = T_k(\tilde{H})$ , where  $\tilde{H}$  is a norm-reduced approximation of  $H$  (which depends on the region decomposition) and  $T_k$  a suitably scaled Chebyshev polynomial of degree  $k$ . The operators  $A_{m,r}^\lambda$  are then computed from a specific decomposition of  $K_m^\lambda$  across the left and right boundaries, yielding  $D^2$  terms  $A_{m,r}^\lambda$  such that the expansion procedure  $V_m^\lambda \rightarrow W_m^\lambda$  described in the main text is guaranteed to have a significant improvement on the viability parameter.

Here we depart from the theoretical algorithm in two important ways. First we use a simpler construction of AGSP, which we expect to exhibit similar behavior but is more efficient to compute. Our AGSP takes the form of an approximation  $K \approx e^{-kH/t}$  obtained by Trotter decomposition. (In Arad *et al.*<sup>1</sup> a similar approach is taken to norm-reduce the parts of the Hamiltonian that lie in the regions  $L, M$  and  $R$  but are a distance at least  $\ell > 0$  from the boundaries.) In Arad *et al.*<sup>1</sup> the properties of the Chebyshev polynomial are essential to establish that the AGSP has sufficiently low bond dimension across the boundaries of region  $M$ . Considering only the efficiency in terms of improvement in viability, however, the use of  $e^{-kH/t}$  over the whole chain gives similar guarantees.

Using our simpler construction implies a loss of theoretical control over the bond dimension  $D$  of the AGSP operator across the left and right cuts. This entails a second main point of departure from the theoretical algorithm, as a choice has to be made as to which operators  $A_{m,r}^\lambda$  to keep. As described in the main text we proceed in a natural way by considering the MPO as an MPS and performing SVD operations to create virtual bonds between sites. We then make the choice of keeping operators associated with the  $D^2$  highest Schmidt weights. This choice is heuristic: the Schmidt weights control the Frobenius norm of the associated term  $A_{m,r}^\lambda$ , rather than the operator norm of the resulting operator, as would be desirable. The heuristic nevertheless proved effective: in practice the magnitude of the Schmidt coefficients often fell off quickly, allowing for a relatively aggressive choice of cutting point.

### 2. Merge process

The second step in the algorithm is called *Merge*. The goal of this step is to combine two neighboring viable sets into a single viable set over the union of the two regions, with similar approximation and size guarantees. The procedure is described as *Merge'* in Arad *et al.*<sup>1</sup>. *Merge'* is provided as input viable sets  $W_m^\lambda$  and  $W_m^{\lambda+1}$  defined over neighboring regions, and returns a viable set

$W_{m+1}^{\lambda/2}$  defined over the union of the two regions. Merge consists of three steps: *Tensoring*, *Random Sampling*, and *Error Reduction*.

1. *Tensoring*: This step is the same as in Arad *et al.*<sup>1</sup>.
2. *Random Sampling*: Here as already mentioned in the main text we depart from Arad *et al.*<sup>1</sup> in an important way. In Arad *et al.*<sup>1</sup> a family of  $s$  vectors lying in  $W_m^\lambda \otimes W_m^{\lambda+1}$  is obtained by random sampling within the subspace. In practice this procedure is very inefficient: (i) it requires performing high-weight (random) linear combinations of MPS, a step that is computationally expensive due to the MPS renormalization procedure; (ii) the linear combinations formed tend to be arbitrary, and in particular their MPS representations may have high MPS bond dimension, as each vector may include an “irrelevant” (with respect to the low-energy eigenspace of the Hamiltonian) component that artificially inflates its complexity.

Here we replace random sampling by a deterministic choice of the  $s$  lowest-energy eigenvectors of the restriction of  $H$  to  $W_m^\lambda \otimes W_m^{\lambda+1}$ . The idea is that low-energy eigenstates are likely, due to the local structure of the Hamiltonian, to display less entanglement. Indeed in practice this procedure is much more efficient, and yields MPS with lower bond dimension, than the random sampling proposed in Arad *et al.*<sup>1</sup>.

However, there is a priori no reason for the low-energy eigenstates of the block Hamiltonian to form a viable set for the global low-energy space. A simple heuristic argument can nevertheless be given to argue correctness of our procedure. Recall that the viability criterion Eq. (1) guarantees that the initial

tensor product space supports a good approximation to any ground state. Considering the Schmidt decomposition of this approximation, each of the Schmidt vectors will have a certain energy with respect to the block Hamiltonian  $H_{m+1}^{\lambda/2}$ , which may not be minimal. The key is thus to argue that vectors with high energy will not have an important contribution to the Schmidt decomposition of the ground state. In general approximation error and energy difference can scale with the norm of the Hamiltonian, making the argument difficult. However, for the purposes of approximating the ground space of a local Hamiltonian two elements play in our favor: first, locality of  $H$ , and second, the area law. The former allows to show that the low-energy space of  $H$  is well-approximated by an approximation of  $H$  with constant norm, so that the error blow-up mentioned above can be controlled (see Arad *et al.*<sup>1</sup>, Proposition 3, for a precise statement). The latter establishes that the ground state has low bond dimension, so that few Schmidt vectors need to be considered (see Arad *et al.*<sup>1</sup>, Lemma 15, for details on how this can be used). Together these two properties provide a heuristic argument in favor of our modified procedure.

3. *Error Reduction*: The goal of this step is to improve the approximation quality of the viable set. We follow the procedure described in Arad *et al.*<sup>1</sup>, except that the operators  $\{A_{m,r}^\lambda\}$  are generated differently, as already described.

The final iteration is performed on two viable sets  $V_{m^*-1}^0$  and  $V_{m^*-1}^1$ , each with support on one half of the system. The algorithm returns the low-lying energies and eigenstates obtained via exact diagonalization of the Hamiltonian restricted to the final viable subspace.